2013

X-ray scattering of a nematic liquid crystal nano-dispersion with negative dielectric anisotropy

A. Lorenz

N. Zimmermann

Satyendra Kumar
Kent State University - Kent Campus, skumar@kent.edu

S. R. Evans

G. Cook

See next page for additional authors

X-ray scattering of nematic liquid crystal nanodispersion with negative dielectric anisotropy [Invited]

Alexander Lorenz,[1] Natalie Zimmermann,[1] Satyendra Kumar,[2] Dean R. Evans,[3] Gary Cook,[4] Manuel Fernández Martínez,[5] and Heinz-S. Kitzerow[1,*]

[1]Department of Chemistry, University of Paderborn, Warburger Str. 100, Paderborn 33098, Germany

[2]Department of Physics, Kent State University, Kent, Ohio 44242, USA

[3]Air Force Research Laboratory, Materials and Manufacturing Directorate, Wright-Patterson Air Force Base, Ohio 45433, USA

[4]Azimuth Corporation, 4134 Linden Avenue, Suite 300, Dayton, Ohio 45432, USA

[5]European Synchrotron Radiation Facility, BP220, Grenoble 38043, France

*Corresponding author: Heinz.Kitzerow@upb.de

Received 17 December 2012; revised 13 February 2013; accepted 22 February 2013; posted 25 February 2013 (Doc. ID 181952); published 9 April 2013

A nematic liquid crystal (LC) mixture was doped with harvested ferroelectric $BaTiO_3$ nanoparticles and investigated with wide- and small-angle x-ray scattering upon heating from the nematic to the isotropic phase. At moderate temperatures, colloidal crystallites were observed. LC test cells with homeotropic anchoring were placed in the x-ray beam and the realignment of the LC director was investigated upon applying an electric field. © 2013 Optical Society of America

OCIS codes: 160.3710, 160.4236.

1. Introduction

Adding ferroelectric nanoparticles to liquid crystals (LCs) has been of great interest [1–5], for example, in achieving asymmetry in the electro-optic response to DC pulses [1], increasing optical diffraction or beam-coupling efficiencies [2,3], influencing the dielectric anisotropy, and influencing phase transition temperatures [4,5]. Recently, it was reported that dispersions of ferroelectric nanoparticles can be prepared by grinding cubic $BaTiO_3$ together with oleic acid as surfactant in a planetary ball mill [6,7] and subsequently harvesting the resultant stressed tetragonal $BaTiO_3$ nanoparticles from a heptane suspension [8]. In spite of extensive descriptions of similar dispersions in the literature [1–5], detailed investigations of the structure of molecular arrangement and its changes under the influence of an electric field are rare. In this work, an LC mixture with negative dielectric anisotropy, EN18 (obtained from Chisso, Japan), was doped with harvested ferroelectric $BaTiO_3$ nanoparticles and studied by x-ray scattering in both capillaries and planar LC test cells.

2. Experimental Procedure

A. Preparation of the Nanoparticle Dispersions and Doping of the LC

First, a dispersion of $BaTiO_3$ nanoparticles with a diameter of ≈15 nm was prepared by grinding cubic (nonferroelectric) $BaTiO_3$ in a planetary ball mill in the presence of oleic acid as a surfactant and heptane as a solvent for 10 h [6]. The precursor $BaTiO_3$ particles, which are cubic as supplied by Aldrich, may be converted into single domain tetragonal $BaTiO_3$ due

1559-128X/13/2200E1-05$15.00/0

to stress induced by the grinding [6,7]—a conversion that will not occur in all of the nanoparticles due to some aggregation. Thus, the nanoparticles that exhibited a strong dipole moment were selectively harvested using a strong electric field gradient as reported in the literature [8]. A dispersion of these particles in pure heptane with a concentration of 3 mg/mL was prepared. The turbid dispersion was stored under continuous stirring with a magnetic stirrer and showed no flocculation over several weeks.

A doped LC sample was prepared with a doping concentration $c_{\text{doping}} = 5$ mg/g. A volume of 0.412 mL of the nanoparticle dispersion was added to 0.25 g of the pure LC in an open glass vessel and subsequently the solvent was allowed to evaporate slowly at ≈50°C under permanent stirring with a magnetic stirrer.

B. Investigations by Small- and Wide-Angle X-ray Scattering

Samples of pure and doped EN18 were investigated by small-angle x-ray scattering (SAXS) and wide-angle x-ray scattering (WAXS) with synchrotron radiation with a wavelength of $\lambda = 1$ Å at beam line ID02 at the European Synchrotron Radiation Facility (ESRF).

The samples were filled into 1.5 mm diameter quartz Lindemann capillaries, sealed with epoxy, and placed inside an Instec hot stage (HCS402) with a precision of 0.1°C. Before the samples were inserted, the hot stage was adjusted to nearly ambient temperature. The capillaries containing the samples were inserted and subsequently centered in the x-ray beam. During the investigation, the samples were slowly heated with a heating rate of 0.2°C/ min in the presence of a magnetic field of ≈2.5 kG. The magnetic field was provided by permanent magnets. The samples were heated to a temperature slightly above the clearing point T_C.

In a second test series, samples of pure and doped EN18 were investigated in LC test cells. Each of these LC test cells was prepared from two indium-tin oxide (ITO)-coated cover slips. Two straps of Mylar film with a thickness of 30 μm were placed onto the ITO layer of the first cover slip. The second cover slip was subsequently placed onto these film spacers. The ITO layers of the two cover slips were assembled face to face. The LC test cells were fixed with epoxy and coated with lecithin in order to provide homeotropic anchoring of the LC. Subsequently, the samples were filled into the LC test cells by capillary forces. With an appropriate cell holder, the test cells were placed in the x-ray beam, providing that the beam was transmitted through the cells in parallel to the surface normal of the cover slips. The cells were addressed with a 500 Hz square-wave signal with variable amplitude (0–10 V). The addressing signal was generated with a frequency synthesizer and a suitable amplifier. The second test series was conducted at ambient temperature.

A scheme of the typical 2D diffraction pattern of a nematic LC is shown in Fig. 1. The pattern shows two sets of rather diffuse reflections. Sharp peaks are unlikely in the 2D diffraction pattern of a nematic LC because only short range order is present. A nematic LC consists of rod-like molecules. On average, these molecules are aligned parallelly. Locally, this alignment can be described by the director. In a LC, the short range order is not as perfect as in a molecular crystal. Moreover, the degree of order decreases with increasing temperature. A scalar order parameter S can be defined as the ensemble average value of the second Legendre polynomial of $\cos^2 \gamma_i$, where γ_i is the angle between the individual molecular axes (i) and the local director [9]:

$$S = 1/2\langle 3 \cdot \cos^2 \gamma_i - 1 \rangle. \tag{1}$$

With the reduced temperature $T_{\text{red}} = T/T_C$, the scalar order parameter can be estimated by the Maier–Saupe theory [9]:

$$S = (1 - 0.98 \cdot T_{\text{red}})^{0.22}. \tag{2}$$

According to Eq. (2), the scalar order parameter exhibits a value of $S \approx 0.42$ at the clearing point and increases with decreasing temperature. The order parameter is limited to values $S < 1$ in the nematic phase. Hence, the characteristic distance of correlation decay D is relatively small in a nematic LC. This leads to a rather broad peak width $\Delta\theta$ of the scattering signal (measured at full width at half-maximum). The peak width decreases with the decrease of the wavelength λ, the increase of the scattering angle θ, and the increase of the characteristic distance of correlation decay [10]:

$$\Delta\theta \approx 0.9 \frac{\lambda}{D \cos(\theta)}. \tag{3}$$

In powder diffraction, the correlation length D corresponds to the average size of microcrystallites. Accordingly, Eq. (3) can be applied to estimate the

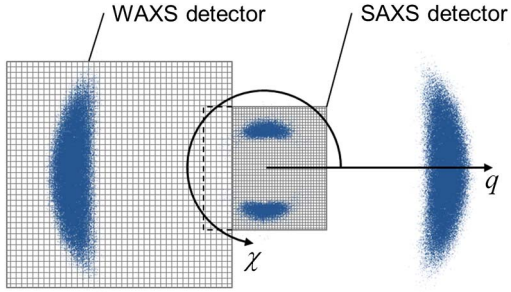

Fig. 1. (Color online) Scheme of the oriented 2D diffraction pattern of a nematic LC, a coordinate system based on the angle χ and the scattering vector q, and the alignment of two detectors, which cover the SAXS and the WAXS angular regions, respectively.

size of microcrystallites D by measuring the peak width $\Delta\theta$.

In the 2D diffraction patterns of LCs, a first set of peaks is observed in the SAXS region. These peaks are caused by scattering due to the intermolecular spacing in the direction parallel to the molecular axes $d_{\parallel}$ [11]. A second set of peaks is observed in the WAXS region. This second set of peaks is caused by scattering due to the intermolecular spacing in the direction perpendicular to the molecular axes $d_{\perp}$.

In the current experiments, the diffraction patterns were recorded using one 2D detector for the WAXS angular region and a second 2D detector for the SAXS angular region (Fig. 1). In order to record data for all relevant scattering angles, the two detectors were carefully adjusted to provide an angular overlap. Thus, a large angular region could be investigated with high resolution.

The 2D diffraction patterns were analyzed with the SAXSutilities software package [12] and MATLAB. The well-known method reported by Davidson *et al.* [13] was applied to estimate the order parameter S by analyzing the peak observed in the WAXS region. In order to apply this method, the nematic LC is required to be aligned homogeneously (with a parallel director field) in the plane perpendicular to the x-ray beam. In the experiments with the quartz Lindemann capillaries, alignment was provided by the permanent magnets. In contrast, an alignment layer and an electric field were used for this purpose in the experiments with the LC test cells.

3. Results

A. Capillaries: Analysis of the Scalar Order Parameter from Scattering in the WAXS Region

Doping was observed to decrease the clearing temperature by 9.2°C from 66.5°C (pure EN18) to 57.3°C (doped EN18). Polarized optical microscopy showed a sharp phase transition in both the pure and the doped samples. The method of Davidson *et al.* [13] yields values of S, that are lower than the values calculated with Eq. (1). For comparison, a theoretical curve S versus T_{red} is shown in Fig. 2 together with the experimental results. As expected, S decreases continuously with T_{red} for pure EN18. However, the curve S versus T_{red} is not perfectly smooth for doped EN18. The scattering intensities observed in the small-angle region (presented in the following section) provide a possible explanation for this unusual behavior.

B. Capillaries: Analysis of Microcrystallites from Scattering in the SAXS Region

For constant values of the scattering vector $q = 4\pi/\lambda \sin\theta$, the detected intensity was integrated over the angle χ (Fig. 1). Figure 3 shows the scattering intensity versus the scattering vector for the doped sample in the temperature range from 29°C to 65°C. Selectively, the SAXS region is shown ($q < 5\ \mathrm{nm}^{-1}$). Three sharp peaks and one overlapping broad peak

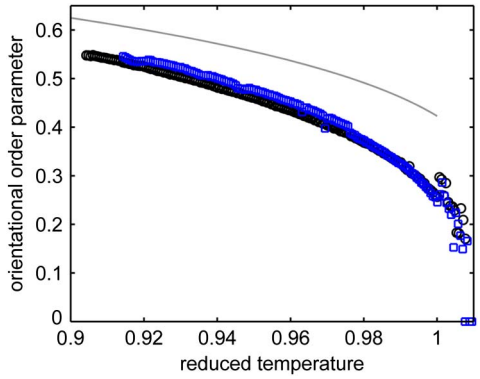

Fig. 2. (Color online) Orientational order parameter versus reduced temperature, as calculated by the Maier–Saupe theory (solid line), observed upon heating pure EN18 (circles) and doped EN18 (squares).

were observed. The broad peak corresponds to the regular scattering of the LC. This broad peak also occurs in the scattering curves of pure EN18 (shown as inset). The peak maximum of the broad peak is located at $q_{\parallel} \approx 3\ \mathrm{nm}^{-1}$, which corresponds to a molecular length of $l \approx 2.1$ nm. The correlation lengths D were analyzed by using the peak width of the broad peak and inserting it into formula (3). This yielded a characteristic length $D_N \approx 9$ nm of the pair correlation function in the nematic phase ($T_{\mathrm{red}} \approx 0.92$) and $D_I \approx 5.6$ nm in the isotropic phase ($T_{\mathrm{red}} > 1$). The three narrow peaks observed in the spectra of the doped sample are centered at $q_1 = 1.367\ \mathrm{nm}^{-1}$, $q_2 = 2.735\ \mathrm{nm}^{-1}$, and $q_3 = 4.101\ \mathrm{nm}^{-1}$. The peaks centered at q_2 and q_3 are second- and third-order Bragg reflections of the structure, which causes the peak to be centered at q_1. The d-spacing of the latter reflection is 4.56 nm, which approximately to twice the molecular length l. The narrow peaks yield a correlation length of $D_{\mathrm{Cr}} \approx 377$ nm. The three peaks are probably caused by microcrystallites. The formation of such crystallites could originate from a

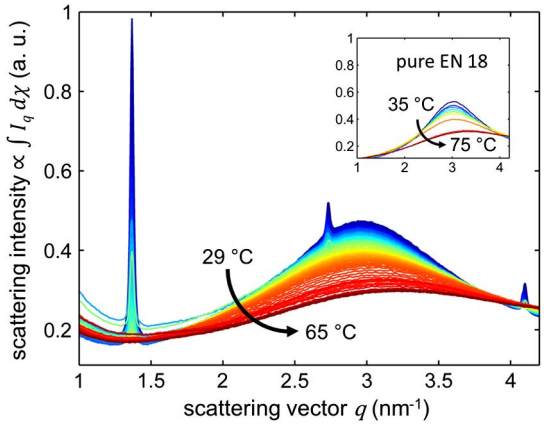

Fig. 3. (Color online) Scattering intensity versus magnitude of the scattering vector recorded for a capillary filled with $BaTiO_3$-nanoparticle-doped EN18. The sample was slowly heated from 29°C (blue curves) to 65°C (red curves). The inset shows scattering curves observed for the pure LC.

reduction of solubility of a compound in the multicomponent mixture EN18. The correlation length in these microcrystallites is one order of magnitude larger than the correlation length of multilayered structures recently observed in nanoparticle-doped 5CB [14]. At low temperatures, these crystallites are dispersed in the nematic LC. Upon heating, the peak maxima decrease, indicating that the number of crystallites decreases with increasing temperature.

C. Electric Field Effects in Planar LC Test Cells

In order to study electric field effects, the LC EN18 and a respective dispersion were filled in homemade planar test cells as described above. Due to the thin lecithin coating, the surface of these cells provides homeotropic anchoring; i.e., the director shows a uniform alignment along the z-direction perpendicular to the substrates [Fig. 4(a)] if $V<V_{cr}$ (in this case $V = 0$). An electric field along the z-direction can be applied by means of conducting transparent electrodes made of ITO. By applying a voltage to the LC test cells, a Fredericks transition can be induced if the voltage exceeds a critical voltage V_{cr} [13]. Since the LC exhibits negative dielectric anisotropy, the director is expected to tilt away from field direction (z-direction) and to align parallel to the substrates [(x,y) plane] for sufficiently high voltages [Figs. 4(b) and 4(c)]. This realignment is known to start in the center of the cell and to propagate toward the substrate with increasing voltage, while the homeotropic alignment of a thin LC layer close to the surface remains preserved. Due to the elastic properties of the LC, the tilt of the director field changes continuously along the z-direction for a voltage $V > V_{cr}$ [Fig. 4(c)].

To study this Fredericks effect, the LC test cells were mounted onto the goniometer of the beam line using an appropriate cell holder. The alignment of the test cells was carefully adjusted to ensure that the incident x-ray beam was propagating along the z-direction (perpendicular to the glass substrates). For 0 V, a large peak centered at $q = 13.5$ nm^{-1} was observed in the WAXS region [Fig. 5(a), gray shaded area] and only weak scattering was observed in the SAXS region (light area). This indicates that only the lateral distance $d_\perp$ of the molecules can be seen in the scattering signal, as expected for homeotropic alignment. However, a SAXS signal appears above

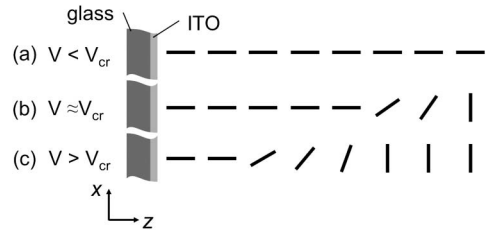

Fig. 4. Fredericks transition in an LC test cell with homeotropic anchoring: schematic plots of the director field near one glass boundary (a) if no voltage is applied (b), if a voltage near the critical voltage is applied, and (c) if a voltage larger than the threshold voltage is applied.

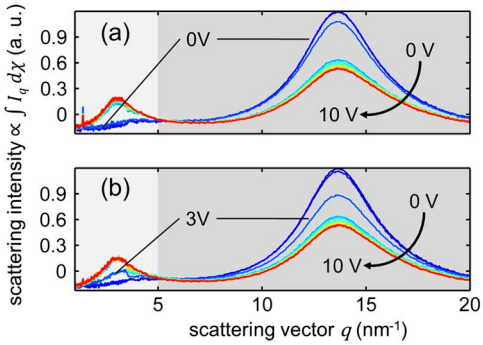

Fig. 5. (Color online) Scattering intensity versus magnitude of the scattering vector recorded for planar LC test cells. The addressing voltage is varied from 0 (blue curves) to 10 V (red curves) in steps of 1 V. (a) Pure EN18. (b) EN18 doped with harvested $BaTiO_3$ nanoparticles.

a critical voltage. It is centered at $q_\parallel \approx 3$ nm^{-1}, indicating again a longitudinal distance $d_\parallel \approx 2.1$ nm of two neighboring molecules, which again corresponds approximately to the molecular length l. A scattering signal at $q = q_\parallel$ is only possible if the director exhibits a nonzero component along the (x,y) plane, perpendicular to the incident x-ray beam. Thus, the first appearance of this peak on increasing voltage indicates the critical value V_{cr}. The critical voltage is between 2 and 3 V for pure EN18 [Fig. 5(a)], but between 1 and 2 V for EN18 doped with nanoparticles [Fig. 5(b)]. This result clearly confirms that adding nanoparticles can reduce the critical voltage V_{cr}, which was also observed in other systems [4,5,1]. The observed reduction in threshold voltage could imply that either the anchoring energy is being lowered by the addition of nanoparticles or the applied field reorients the ferroelectric nanoparticles, which, in turn, due to their ferroelectric nature, enhance the local electric field and thus promote the reorientation of the LC. The exact mechanism of this change is not clear at this time. However, the changes of the x-ray signals on increasing voltage are in agreement with our expectations: while the SAXS signal increases with increasing voltage, indicating the increasing tilt of the director away from the z-direction, the intensity of the WAXS signal decreases. A detailed analysis of the director field from these signals will be elaborate and is beyond the scope of this paper, because the director alignment is not uniform, but changes continuously along the propagation direction of the x-ray beam (Fig. 4). However, this preliminary study encourages further studies in this direction.

Angular scans (varying the angle χ) of the detected intensity in the WAXS region are shown for a test cell filled with pure EN18 [Fig. 6(a)] and doped EN18 [Fig. 6(b)], respectively. In these scans, a straight line is observed at 0 V, because the director field is oriented homogeneously in parallel to the transmission direction of the x-ray beam, throughout the whole cell. Accordingly, the radiation is scattered with equal probability for all angles χ in the initial state.

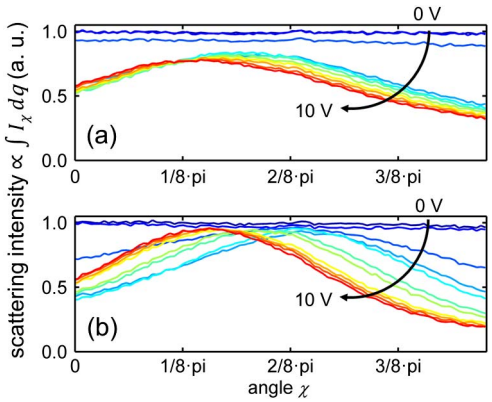

Fig. 6. (Color online) Angular scans of the scattering intensity (integrated over q in the WAXS region) versus angle χ.

In contrast, the angular scans show a curved shape at higher voltages because the director field is—at least partially—realigned in a direction perpendicular to the beam. Consequently, the integral scattering is reduced and the WAXS signal shows the typical shape observed for oriented samples of nematic LCs. The preliminary data shown in Fig. 6 seem to indicate that the voltage-induced azimuthal alignment of the director is more uniform in the doped sample [Fig. 6(b)] than in pure EN18 [Fig. 6(a)]. However, any conclusion would be premature, because all azimuthal directions in the (x, y) plane perpendicular to the field are degenerate. Just by accident, the beam diameter might cover either many domains with different azimuthal orientations or few domains with similar azimuthal orientations. So, more detailed investigations are necessary.

4. Conclusions

Relatively large molecular crystallites with a size of ≈380 nm were observed in a nematic LC doped with ferroelectric nanoparticles. The microcrystallites consisted of molecular bilayers. However, the dispersion of the microcrystallites was destabilized upon heating and microcrystallites were also present in the pure sample at room temperature. If the nanoparticles lead to a stabilization of the microcrystallites or to a partial crystallization of the LC, the composition of the LC mixture could be changed. This could be an explanation for the observed decrease in the clearing temperature.

The director reorientation of an LC with negative dielectric anisotropy could be studied by x-ray scattering in LC test cells. This is remarkable, because only a thin layer of the LC with a thickness of ≈30 μm is investigated in the test cells, while the Lindeman capillaries have a diameter of 1.5 mm. Also, the capillaries have a wall thickness of only 10 μm, whereas the cover slips have a thickness of ≈100 μm. Although the glasses of the LC test cells are much thicker than the walls of the capillaries, the LC realignment could be studied well with synchrotron radiation. An LC nanodispersion with ferroelectric nanoparticles showed a more pronounced reorientation and a reduced threshold voltage as compared to an undoped LC. For more detailed analysis, further studies are necessary.

The authors thank Theyencheri Narayanan (ESRF) for helpful discussions. Support by the German Research Foundation (KI 411/14 and GRK 1464), the European Science Foundation (EUROCORES, SONS II, "Self-organized nanostructures"), the European Synchrotron Radiation Facility (ESRF) proposal HD-538, and (SK by) the U.S. Department of Energy, Basic Energy Sciences grant DE-SC0001412, is gratefully acknowledged.

References

1. G. Cook, V. Yu. Reshetnyak, R. F. Ziolo, S. A. Basun, P. P. Banerjee, and D. R. Evans, "Asymmetric Freedericksz transitions from symmetric liquid crystal cells doped with harvested ferroelectric nanoparticles," Opt. Express **18**, 17339–17345 (2010).
2. O. Buchnev, A. Dyadyusha, M. Kaczmarek, V. Reshetnyak, and Y. Reznikov, "Enhanced two-beam coupling in colloids of ferroelectric nanoparticles in liquid crystals," J. Opt. Soc. Am. B **24**, 1512–1516 (2007).
3. G. Cook, A. V. Glushchenko, V. Reshetnyak, A. T. Griffith, M. A. Saleh, and D. R. Evans, "Nanoparticle doped organic–inorganic hybrid photorefractives," Opt. Express **16**, 4015–4022 (2008).
4. A. Glushchenko, C. I. Cheon, J. West, F. Lic, E. Büyüktanir, Y. Reznikov, and A. Buchnev, "Ferroelectric particles in liquid crystals: recent frontiers," Mol. Cryst. Liq. Cryst. **453**, 227–237 (2006).
5. F. Li, O. Buchnev, I. C. Cheon, A. Glushchenko, V. Reshetnyak, Y. Reznikov, T. J. Sluckin, and J. L. West, "Orientational coupling amplification in ferroelectric nematic colloids," Phys. Rev. Lett. **97**, 147801 (2006).
6. H. Atkuri, G. Cook, D. R. Evans, C.-I. Cheon, A. Glushchenko, V. Reshetnyak, Y. Reznikov, J. West, and K. Zhang, "Preparation of ferroelectric nanoparticles for their use in liquid crystalline colloids," J. Opt. A **11**, 024006 (2009).
7. S. A. Basun, G. Cook, V. Yu. Reshetnyak, A. V. Glushchenko, and D. R. Evans, "Dipole moment and spontaneous polarization of ferroelectric nanoparticles in a nonpolar fluid suspension," Phys. Rev. B **84**, 024105 (2011).
8. G. Cook, J. L. Barnes, S. A. Basunm, D. R. Evans, R. F. Ziolo, A. Ponce, V. Y. Reshetnyak, A. Glushchenko, and P. P. Banerjee, "Harvesting single ferroelectric domain stressed nanoparticles for optical and ferroic applications," J. Appl. Phys. **108**, 064309 (2010).
9. W. H. de Jeu, *Physical Properties of Liquid Crystalline Materials* (Gordon & Breach, 1980).
10. P. Scherrer, "Bestimmung der größe und der inneren struktur von kolloidteilchen mittels röntgenstrahlen," Göttinger Nachrichten Math. Phys. **2**, 98–100 (1918).
11. W. L. McMillan, "Simple molecular model for smectic a phase of liquid crystals," Phys. Rev. A **4**, 1238–1246 (1971).
12. SAXSutilities is a piece of software developed by Michael Sztucki, July 2011, ESRF.
13. P. Davidson, D. Petermann, and A. M. Levelut, "The measurement of the nematic order parameter by x-ray scattering reconsidered," J. Phys. II **5**, 113–131 (1995).
14. A. Lorenz, N. Zimmermann, S. Kumar, D. R. Evans, G. Cook, and H.-S. Kitzerow, "Doping the nematic liquid crystal 5CB with milled $BaTiO_3$ nanoparticles," Phys. Rev. E **86**, 051704 (2012).